Elastic Instability in Growing Yeast Colonies

Baochi Nguyen,* Arpita Upadhyaya,† Alexander van Oudenaarden,† and Michael P. Brenner‡
Department of *Mathematics and †Physics, Massachusetts Institute of Technology, Cambridge, Massachusetts; and ‡Division of Engineering and Applied Sciences, Harvard University, Cambridge, Massachusetts

ABSTRACT The differential adhesion between cells is believed to be the major driving force behind the formation of tissues. The idea is that an aggregate of cells minimizes the overall adhesive energy between cell surfaces. We demonstrate in a model experimental system that there exist conditions where a slowly growing tissue does not minimize this adhesive energy. A mathematical model demonstrates that the instability of a spherical shape is caused by the competition between elastic and surface energies.

INTRODUCTION

The differential adhesion hypothesis states that cells in a growing tissue organize themselves to minimize the surface energy associated with the adhesion of different cells to each other. The hypothesis assumes that an aggregate of cells with different adhesive strengths is similar to a system of different liquids with different surface tensions. Over the years, many studies have provided evidence for this hypothesis via both experiments (Fink and McClay, 1985; Foty et al., 1994, 1996; Ryan et al., 2001; Steinberg, 1962, 1964; Townes and Holtfreter, 1955; Trinkaus, 1963) and simulations (Glazier and Graner, 1993; Palsson and Othmer, 2000). The surface tension of certain embryonic tissues have been directly measured (Foty et al., 1994, 1996), and as expected, mixtures of cells segregate to minimize the overall surface energy.

If the morphology of a growing tissue is dictated solely by surface energy minimization, then this has implications not only for the position of cells relative to each other but also for the overall shape of the tissues: in the absence of external forces, a tissue-minimizing surface energy should be composed of spherical regions. The goal of the present work is to test this hypothesis within a particularly simple example: the shape of a droplet of a single cell type growing on a nutrient-enriched substrate. As for liquid droplets, the equilibrium shape of such a structure is a spherical cap with a contact angle given by Young's law,

$$\gamma_{CA}\cos(\theta) + \gamma_{CS} = \gamma_{SA}, \tag{1}$$

which relates the equilibrium contact angle θ of the colony at the agar substrate to the surface energies of the liquid and solid. Here, γ_{CA} is the adhesion energy of the cells to each other, γ_{CS} is the adhesion energy of the cells to the substrate, and γ_{SA} is the energy per unit area of the substrate. All of these quantities should change when the types of cell and substrate are varied.

Our experiments focus on colonies of Baker's yeast (*Saccharomyces cerevisiae*), growing on an agar substrate. The advantage of this system is threefold. First, the gene expressing the adhesive protein (FLO11) is known, and thus the cell-cell adhesion γ_{CA} can be genetically controlled. Second, the adhesivity of the substrate γ_{CS} can be varied by changing the agar concentration. Third, yeast cells are spherical and have no mechanism for active motility. The experiments demonstrate that, consistent with Young's law (Eq. 1), changing either the agar concentration or the expression of FLO11 modifies the local contact angle of the yeast droplet. Moreover, when the colony is sufficiently small, its shape is a spherical cap, consistent with surface energy minimization. However, above a critical (contact-angle-dependent) volume the spherical structure is unstable, and the colony develops a nonspherical shape. Since these shapes are inconsistent with surface energy minimization, the experiments demonstrate that there must be other forces acting on the tissue. The possible candidates in our experiments are gravity, adhesive gradients, growth stresses, and elastic stresses. We present a mathematical model suggesting that the change in tissue morphology arises from elastic deformations of the colony. The model demonstrates that a spherical elastic droplet on a solid substrate with fixed contact angle is unstable above a critical (contact-angle-dependent) volume, quantitatively consistent with experiments. The model reproduces both the instability threshold and the shape of the yeast droplets near the threshold, consistent with the experiments.

The organization of this article is as follows. In Experimental Procedures, we describe our experimental system and discuss the results. A phase diagram is presented delineating the borderline between spherical shapes (where the colony shapes minimize surface energy), and nonspherical shapes (where other forces are acting). In Mathematical Model, we derive a mathematical model for an elastic droplet on a solid surface, and analyze the stability of the droplet to nonspherical perturbations. The instability threshold is computed and compared with experimental observations. We also present analytic calculations of droplet

Submitted June 12, 2003, and accepted for publication January 6, 2004.

Address reprint requests to Professor Michael P. Brenner, Division of Engineering and Applied Sciences, Harvard University, 29 Oxford St., Cambridge, MA 02458. Tel.: 617-495-3336; E-mail: brenner@deas.harvard.edu.

0006-3495/04/05/2740/08 $2.00

shapes beyond the transition. Finally, Discussion presents conclusions and directions for future work.

EXPERIMENTAL PROCEDURES

Background

Our study focuses on an assay discovered by Reynolds and Fink (2001). They noticed that when Baker's yeast (*S. cerevisiae*) grows in a low glucose medium they adhere to plastic and form biofilms. The ability of the yeast to stick to plastic was traced back to FLO11, a yeast gene encoding a cell surface glycoprotein that allows cells to adhere to agar and to each other. This gene can be turned off (producing the mutant flo11Δ) or overexpressed (producing the strain sfl1Δ), so that three independent strains of otherwise identical cells with different adhesion strengths exist. Reynolds and Fink found that when wild-type (WT) yeast grows on a low agar concentration (0.3%), it forms a complex structure with reproducible features. Since the cells are nonmotile, the structures that form are entirely the result of the forces that act upon them. The morphologies observed in the Reynolds-Fink experiments are determined by a large number of related effects, including adhesion, nutrient consumption, and water content.

Materials and methods

Yeast strains

We use Baker's yeast *S. cerevisiae* with different levels of expression of the adhesive protein FLO11 (obtained from the laboratory of Dr. G. Fink, The Whitehead Institute, Cambridge, MA). There are three strains, flo11Δ, wild-type (WT), and sfl1Δ, that express low (zero), normal, and high levels of FLO11, respectively. The strains are characterized by the levels of adhesion as nonsticky, sticky, and supersticky. The system has many advantages. First, these cells are spherical and nonmotile with an average cell division time of 2 h. Cellular rearrangements are possible through forces the cells exert on each other and on their environment. An aggregate of these cell types has an effective surface energy γ_{CA} due to adhesive interactions between individual cells. The magnitude of γ_{CA} is set by the concentration of this cell surface protein, which is genetically controlled.

Preparation of agar substrate and yeast colonies

The growth medium YPD is composed of water, 1% Difco yeast extract, 2% Bacto peptone, and 2% Mallinckrodt dextrose. A desired amount of Bacto agar is added to the growth medium. The mixture is then autoclaved for 20 min at 122°C to dissolve the agar and sterilize the medium. The substrate is prepared by pouring 30 ml of the sterile mixture into a sterile petri dish (Corning, Acton, MA) and allowed to set for 1 h. A sterilized glass plate is placed at the bottom of the petri dish before pouring in the mixture. This makes the transfer of the substrate between the petri dish and the microscope stage more stable and easier. When the plates are set, they are ready for inoculation. Colonies are inoculated by spreading 25 μl of a dilute mixture of yeast cells and liquid YPD. The inoculation procedure ensures that for each plate the number of colonies is small (<20) and spread out. The inoculated plates are placed in a humidified incubator at 28° for a couple of days.

Imaging and data analysis

Once the colonies are visible by eye the imaging process begins with a side-view microscope (Leica Monozoom 7, Leica, Bannockburn, IL) with an attached charge-coupled device camera. This allows the measurement of contact angles that a yeast colony makes with the agar substrate and the two-dimensional shape of the colony as a function of time. For imaging, the glass plate with the agar substrate is cut and removed from the petri dish and then placed on the microscope stage. A dual cold light source (Fiber Lite MI-150, Dolan Jenner, Lawrence, MA) is used to illuminate the colonies from the sides. Time-lapse images of the colonies on the same plate are taken every few hours; between images the plates are placed back in a humidity controlled environment. Even with the glass plate, the transferring of a substrate of agar concentration $<1\%$ is not stable. This limits the experiments to agar concentrations of $\geq 1\%$. We acquire and analyze the images using Metamorph software (Universal Imaging, Downington, PA).

Results

Contact angle

The first set of experiments is designed to measure the contact angle of a yeast droplet for fixed agar concentration, and to determine if it remains constant throughout the growth of the colony, as implied by Eq. 1. Time-lapse images of colonies of the same plate were taken every 2 h. Our initial experiments showed that although the shape of small yeast droplets remains spherical, the contact angle actually increases with time, contradicting Young's law with constant surface energies. We hypothesized that the increase in the angle might arise from the evaporation of water from the colonies and the substrate during the imaging process. We therefore conducted a set of experiments using a number of identically inoculated plates to verify this hypothesis. After the colonies on a given plate are imaged, the plate is discarded to avoid evaporation. Images at later times were taken from a fresh plate from the incubator. These experiments demonstrate that the contact angle remains constant during the entire growth of the colony (Fig. 1). The con-

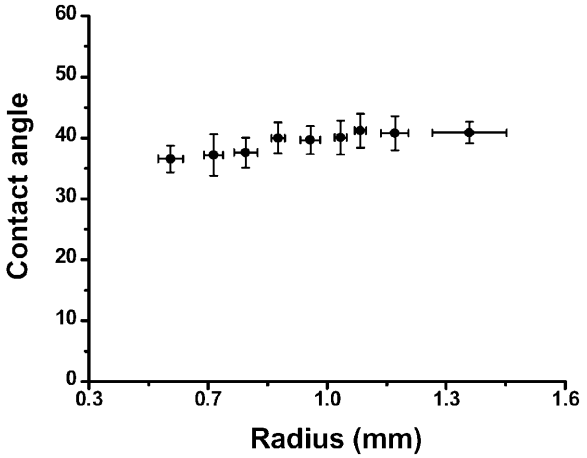

FIGURE 1 Constant contact angle. Plot of contact angle as a function of radius of WT colonies on 2.1% agar concentration. Each point is an average of 20 colonies. Images taken were then sorted according to size. Error bars represent the standard deviation.

stancy of the contact angle is obeyed even after the instability (to be discussed subsequently) occurs.

Fig. 2 shows images demonstrating that an increase in cell-cell adhesion increases the contact angle. The super-sticky Sfl1Δ strain has the highest contact angle at a given agar concentration, consistent with its higher surface tension. The sticky wild-type (WT) and nonsticky flo11Δ strains have similar contact angles. Although one might expect the wild-type strain to have a larger contact angle than the mutant flo11Δ strain owing to the expression of the adhesive protein, this neglects the effect of water on the surface energy of the colony. When the adhesion between cells is sufficiently weak, one would expect the cell-cell adhesion energy γ_{CA} to be dominated by the surface tension of water; although we have no direct way of measuring γ_{CA}, we believe this is a consistent interpretation of the data.

Fig. 2 also shows images documenting the change in θ on varying the agar concentration from 1% to 3%. The contact angle increases with increasing agar concentration. The mechanism through which the yeast colony adheres to the agar is unknown. If the yeast cells adhered to the agar directly, one would expect the contact angle to decrease with increasing agar concentration. This is because higher agar concentrations would give a higher concentration of binding sites between the yeast and agar, consequently changing γ_{CS}. On the other hand, increasing agar concentration also visibly dehydrates the yeast colony; this effect will also change the cell-cell surface energy γ_{CA}.

Although the molecular mechanisms controlling the contact angle are interesting, the most important conclusion for the present study is that the contact angle remains constant in time, and can be manipulated by changing either the agar concentration or the cell adhesion.

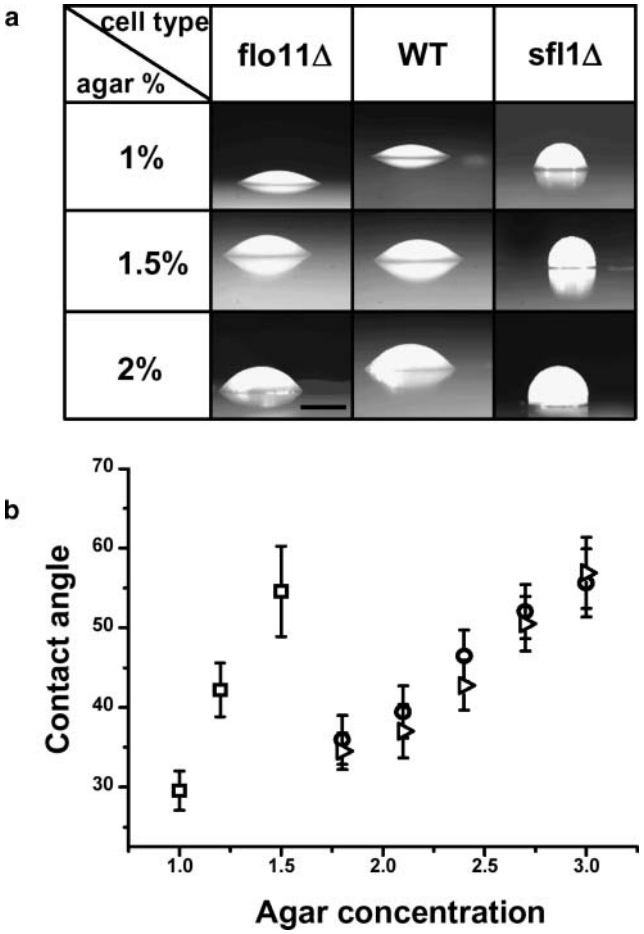

FIGURE 2 Dependence of contact angle on adhesion and agar concentration. (*a*) Side view of colonies from three strains on substrate of different agar concentrations. Increasing cell adhesion is horizontally across and increasing agar concentration is vertically down. (*b*) Plot of contact angle as a function of agar concentration for sfl1Δ (*squares*), WT (*circles*), and flo11Δ (*right triangles*). The scale bar denotes 100 μm.

Colony shape

When the colony is sufficiently small, the shape is always a spherical cap, as expected from surface energy minimization. However, we observe that at a critical time during the growth, the spherical shape destabilizes. After the instability, the resulting morphologies include staircase, staircase with centered dimple, and spherical cap with dimple (Fig. 3). A contour plot of time-lapse images of a WT colony (Fig. 4) demonstrates the transition of the colony from spherical to nonspherical. Extensive observations indicate that the character of the instability is determined entirely by the contact angle θ. For instance, a superadhesive sfl1Δ colony on 1.5% agar concentration has a similar contact angle to a wild-type colony on 2.1% agar; although the surface tension γ_{CA} of sfl1Δ is higher than the wild-type, the Young's law equation (Eq. 1) implies that this is compensated by the higher agar concentration. Despite the differing

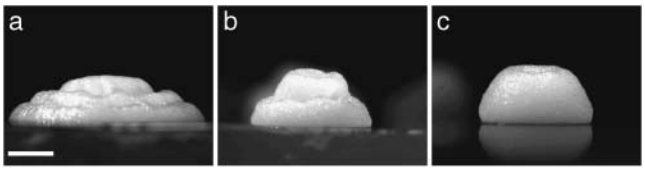

FIGURE 3 Types of instabilities. Images of the different types of unstable morphologies from WT (*a*) and sfl1Δ (*b*, *c*) on 1.8, 1.2, and 2% agar concentrations, respectively. The three types of morphologies imaged are staircase (*a*), staircase with dimple (*b*), and dimple (*c*). The scale bar denotes 1 mm.

mechanisms leading to the contact angle, both types of colonies come to a staircase morphology. This suggests that morphology is controlled completely by the adhesion level and agar concentration, which together determine the contact angle of the colony.

This observation suggests that the critical volume where a nonspherical shape occurs can only depend on the contact angle, θ, with no explicit dependence on the type of cells or the agar concentration. To test this hypothesis we measured a phase diagram (Fig. 5) of colony morphologies as a function of colony volume and contact angle. The transition to nonspherical shapes indeed occurs above a contact-angle-dependent critical volume. In Fig. 5, for high contact angles and low colony volumes, the shapes are spherical; for low contact angles and high colony volume, the shapes are nonspherical. The nonspherical regime is divided into three subregimes based on the contact angle: at low angles ($\theta < 40°$), the shapes are staircases; at midangles they are staircases with a dimple; at highest angles ($\theta > 70°$), they are dimples.

The experimental phase diagram is obtained with the WT and flo11Δ strains on four different agar concentrations ranging from 1.8% to 3% and sfl1Δ strain on 1–1.5%. For each agar concentration, we make eight identical plates. Images are taken from a different plate every 2 h. At the end of the experiment we have ~150 images per agar concentration. The detected edge $y^{\text{expt}}(x_i)$, $\{i = 1 \ldots N\}$ is analyzed to obtain contact angles, radii, and areas of the

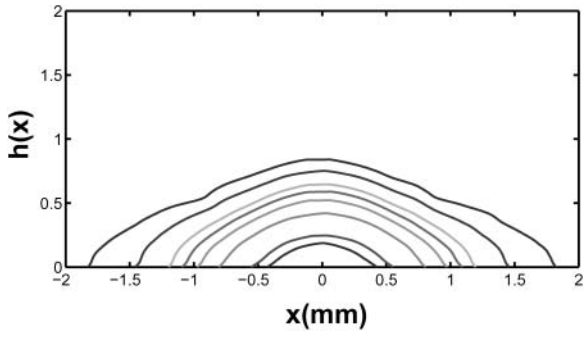

FIGURE 4 Contour plot of time-lapse images of a WT colony on 2.1% agar concentration. Two hours elapse between each two contours starting from the innermost curve.

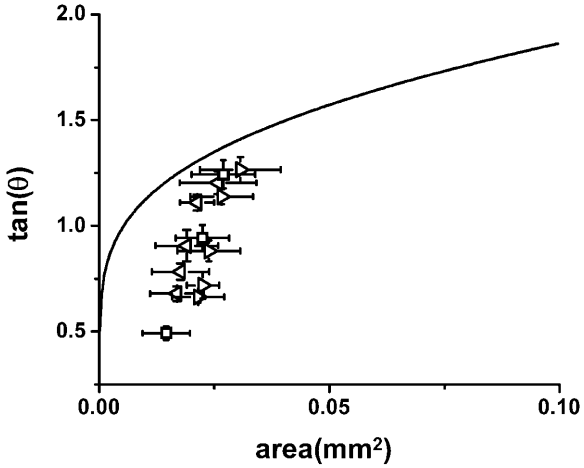

FIGURE 5 Theoretical (*solid line*) and experimental (*points*) phase diagram. The bifurcation curve demonstrates when the transition from spherical to nonspherical shape occurs. Above the theoretical curve is the spherical regime and below is the nonspherical regime. Experimental data come from WT colonies (*left triangles*) and flo11Δ (*right triangles*) on 1.8, 2.1, 2.4, 2.7, and 3% agar concentrations, as well as sfl1Δ (*squares*) on 1, 1.2, and 1.5% agar.

colonies. The edges are then fit to a circular cap $y^{\text{fit}}(x)$ using a least-squares method. We then calculate χ^2, defined as

$$\chi^2 = \frac{1}{N}\sum_{i=1}^{N}\frac{(y^{\text{fit}}(x_i) - y^{\text{expt}}(x_i))^2}{\sigma^2},$$

where σ is the measurement error per data point. When the colony transitions from a spherical to a nonspherical shape, χ^2 rapidly increases. We are interested in detecting the early stage of the instability. We define the instability to occur when χ^2 is in the range between 0.1 and 0.3. Applying this threshold to each set of conditions then yields the phase diagram (Fig. 5).

The fact that the spherical colony shape destabilizes above a critical volume implies that there must be a force other than surface tension affecting the colony shape. The obvious candidates for this additional force are gravity, gradients in adhesivity caused by nonuniform nutrient consumption or waste production in the colony, and elastic stresses. Although gravitational forces should play a role when the colony is sufficiently large, we ruled out gravity by performing experiments on colonies grown while inverted. The colony becomes unstable at exactly the same volume independent of its orientation relative to gravity. We tested for the importance of nutrient consumption or waste production by carrying out experiments where the glucose level in the substrate is varied. Since the expression of adhesive protein is directly controlled by the level of glucose (Reynolds and Fink, 2001), varying the glucose level simulates the effect of nutrient consumption. The experiments showed that the instability occurs at the same critical

volume for different levels of glucose, ruling out the possibility of nutrient depletion on causing the instability.

The only remaining candidate is the possibility of developing elastic stresses in the colony. Elastic stresses might be generated by cell growth; however, the very slow cell division timescale (typically 2 h) makes this unlikely. Assuming the colony material is similar to particulate gel, we can compare the growth rate to the stress relaxation rate. Yeast cells divide on average every 90 min; hence, the growth rate is 1/5400 s^{-1}. The shear modulus of a particulate gel of volume fraction ≈ 0.5 is of $\sim 10^3$dyn/cm^2 and the maximum dynamical viscosity is of $\sim 10^2$ dyn/s per cm^2 Larson (1999); hence, the stress relaxation rate is $\sim 10\ s^{-1}$, which is much larger than the growth rate. Therefore, the elastic stresses induced by cell growth relax very quickly, and should not affect the colony morphology. Elastic stresses might also arise due to a direct instability of the spherical cap, in which the elastic energy to support a nonspherical shape is less costly than the surface energy for the shape to remain spherical. To explore this possibility, we developed a phenomenological mathematical model of an elastic droplet on a solid surface. The model demonstrates that the spherical cap solution is unstable at a contact-angle-dependent critical volume, reminiscent of the experimental findings.

MATHEMATICAL MODEL

To assess the possibility of an elastic instability of the yeast colony, we study the stability of a spherical cap with fixed contact angle to nonspherical perturbations, assuming that the total energy is the sum of surface and elastic energies. The calculation we carry out here is actually two-dimensional, for the interests of algebraic simplicity; hence the term ''spherical cap'' refers to an infinite two-dimensional cylindrical cap. The strategy of our stability analysis is as follows: first, we assume that the shape of the colony with fixed volume and fixed contact angle is $h(x)$, not necessarily a spherical cap. Here $h(x)$ denotes the thickness of the colony a horizontal distance x from its center. We then compute the elastic stresses that are necessary for this shape to be in equilibrium, assuming that the elastic stresses balance the capillary pressure from the unbalanced surface tension force. Finally, the total energy (surface and elastic) is minimized, subject to constant volume and constant contact angle constraints that give the preferred shape of the colony. We view this calculation as phenomenological, since the precise mechanism coupling capillary forces to elastic stresses is not specified.

Elastic lubrication theory

We begin by calculating the elastic strain that must exist in the colony for a nonspherical shape to remain in equilibrium. We consider a two-dimensional colony with height $z = h(x)$. The strain field in the colony is $\nabla\mathbf{u}(x, z)$ where $\mathbf{u}(x, z)$ is the displacement. For small deviations from a spherical cap (for which there are no elastic strains) we assume the displacement field is measured relative to the spherical cap with identical volume. The yeast colony is incompressible ($\nabla \cdot \mathbf{u} = 0$), owing to the water in the yeast droplet. Displacements in the colony then follow from the equilibrium equations of an elastic droplet,

$$G\nabla^2\mathbf{u} + \nabla\mathbf{p} = 0, \tag{2}$$

$$\nabla \cdot \mathbf{u} = 0, \tag{3}$$

where G is the elastic modulus of the material (Landau and Lifshitz, 1986). We remark that the magnitude of G is not the same as the elastic modulus of a single yeast cell (Smith et al., 2000), since the elastic deformations of a yeast colony result in deformation of the network of cells in the colony, instead of the individual cells themselves (Larson, 1999). The bulk elasticity G is therefore much smaller than that of the cells themselves. A typical value of G for particulate gel is $\sim 3 \times 10^3$ dyn/cm^2 for a volume fraction of 0.5 (Larson, 1999).

To compute the strain predicted by Eqs. 2 and 3, we assume that the characteristic length scale of the colony in the horizontal (x) direction, L, is much larger than that in the vertical (z) direction, h. Such a lubrication approximation is common in analyzing thin-film flows in fluid mechanics (Batchelor, 1973). Denoting the components of the displacements $\mathbf{u}$ in the x and z directions as u_x and u_z, respectively, the equilibrium equations are

$$G\nabla^2\mathbf{u} \approx G\frac{\partial^2\mathbf{u}}{\partial z^2} = -\nabla p, \tag{4}$$

where we have used the fact that the horizontal scale is much larger than the vertical scale to approximate $\partial_x^2 \ll \partial_z^2$. Similarly, the incompressibility condition $\partial_x u_x + \partial_z u_z = 0$ implies $u_z = -z(\partial u_x/\partial x) + \ldots$, so that $[u_z] \sim h/L[u_x]$. Hence when $h/L \ll 1$ we have $u_z \ll u_x$, and vertical displacements are unimportant. Similarly, Eq. 4 implies that $\partial_z p \ll \partial_x p$, so that we can assume the pressure primarily depends on the horizontal coordinate $p = p(x)$.

With these simplifications the equilibrium equations reduce to a single equation for u_x. Henceforth we drop the subscript x and denote the elastic displacement by u. The boundary conditions are that the displacement vanishes on the agar substrate $u(z = 0) = 0$, and the shear stress at the yeast-air interface vanishes $\partial_z u(z = h) = 0$; finally, the pressure at the yeast-air interface is given by the Gibb's condition (Landau and Lifshitz, 1987),

$$p(z = h) = -\gamma h''. \tag{5}$$

This last equation provides the coupling of the surface tension force to the elasticity stresses; although the coupling

appears to be benign, coinciding as it does with the classical Gibb's condition at liquid-liquid interfaces, the equation must be viewed as phenomenological. In particular, at this level of description we are not specifying the precise mechanism through which capillary forces create elastic stresses. We will comment more on this issue later in the article.

Applying the boundary conditions and solving Eq. 4 gives the displacement in terms of $h(x)$,

$$u = \frac{\gamma h'''}{G}\left[\frac{z^2}{2} - zh\right]. \tag{6}$$

A straightforward calculation then gives the total energy of a yeast colony with arbitrary shape $h(x)$,

$$E[h] = \frac{2\gamma^2}{3G}\int h'''^2 h^3\,dx + \gamma\int\sqrt{1+h'^2}\,dx + p_0\int h\,dx, \tag{7}$$

where the first term is the elastic energy, the second term the surface energy, and p_0 is a Lagrange multiplier (''pressure'') that enforces the constant volume constraint. Note that if the shape is exactly a spherical cap (so that $h(x) = h_0(x)$ has constant curvature), the elastic energy vanishes identically, so the spherical cap solution is a stationary solution to Eq. 7.

Instability of spherical cap

Our goal now is to demonstrate that there are colony shapes with a fixed volume v_0 and equilibrium contact angle θ that can lower their energy by deviating from a spherical cap. We first give a qualitative argument exposing how this instability can arise, and then proceed with a detailed calculation.

Scaling argument

Consider a colony with volume v_0 and contact angle θ. If h is the characteristic thickness of the colony and R is its radius, then $v_0 \sim hR \sim R^2\theta$. From Eq. 7, the elastic energy of such a colony is of order $(\gamma^2/\mathrm{G})(\mathrm{h}/\mathrm{R}^3)^2h^3R \sim (\gamma^2/\mathrm{G})\theta^5$ and the surface energy is of order $\gamma(\mathrm{h}/\mathrm{R})^2R \sim \gamma\theta^2R$. At large enough radius, the surface energy contribution dominates the elastic energy, and thus the colony will deform. These two energies are the same order of magnitude when $\theta^* \sim (G/\gamma R^*)^{1/3}$ or $\theta^* \sim ((G/\gamma)^2v_0^*)^{1/7}$, where γ/G is the characteristic length scale representing the competition between surface tension and elasticity. For a typical yeast colony, $\gamma \sim 10$ dyn/cm (Forgacs et al., 1998) and $G \sim 3 \times 10^3$ dyn/cm^2 (Larson, 1999) so the characteristic scale of the instability is 10^{-2} cm. For volumes $v_0 > v_0^*$ an instability to a nonspherical solution will occur. Note that in this regime, increasing the volume of the colony increases both the elastic and surface energies. However, it is cheaper overall to distort the surface then to spread the colony into the larger area necessary to maintain constant contact angle.

Quantitative argument

The scaling argument can be made quantitative by studying the first variation of Eq. 7. Assuming that $h' \ll 1$, we have

$$\frac{2\gamma^2}{3G}\left[-(h'''h^3)''' + 3h'''^2h^2\right] - \gamma h'' = p_0. \tag{8}$$

We are interested in solutions to Eq. 8 that are close to a spherical cap. Denote $h_0(x) = (2\mathrm{v}_0/3\mathrm{R})(1 - x^2/R^2)$ as a spherical cap with radius R and volume v_0. The radius is related to the contact angle through $\tan(\theta) = (4\mathrm{v}_0/3\mathrm{R}^2)$, and the pressure enforcing the volume constraint is then $p_0 = (4\gamma/3\mathrm{R})$. Taking $h = h_0 + c\rho$ and expanding Eq. 8 to leading order in ρ and integrating twice, we obtain

$$(h_0^3\rho''')' + \alpha\rho = 0, \tag{9}$$

where $\alpha = 3G/2\gamma$. A nonspherical solution exists if there exist nonzero solutions to Eq. 9, satisfying the boundary conditions. The boundary conditions are that the solution is symmetric around the origin $\rho'(0) = \rho'''(0) = 0$; at the radius R the profile vanishes $\rho(x = R) = 0$ and the slope obeys the contact angle condition $(-4\mathrm{v}_0/3\mathrm{R}^2) + \rho'(x = R) = -\tan\theta$. (For the spherical cap solution, $\rho = 0$, so the radius satisfies $R = \sqrt{4v_0/(3\tan(\theta))}$.) Finally, since we are considering perturbations to the shape at constant volume, if we fix the volume of the solution to be v_0, then the volume associated with ρ must vanish ($\int_{\mathrm{x}=0}^{\mathrm{R}}\rho\,dx = 0$). The boundary conditions correspond to five conditions on the solution; Eq. 9 is fourth order, and in addition we have the unknown critical volume v_0^*. Hence these conditions are sufficient to uniquely specify the instability.

The most convenient way to find additional solutions is to rescale the horizontal coordinate $y = x/R$, and introduce $v' = \rho$. The volume constraint on ρ then implies that $v(y = 0) = v(y = 1) = 0$. The equation for v is

$$[(1 - y^2)^3v'''']' + \Gamma v' = 0, \tag{10}$$

with boundary conditions $v''(0) = v''''(0) = v(0) = v(1) = v'(1) = 0$. Now we can view $\Gamma = \alpha 2R^4/3v_0$ as an eigenvalue. We numerically computed the smallest eigenvalue for which nonzero solutions to this equation exist: $\Gamma = \Gamma^* = 65.12$. Hence, we have an explicit formula for the bifurcation curve, $\tan\theta^* = 0.72((\gamma/G)^2v_0^*)^{1/7}$. Notice that γ/G is a characteristic length scale. Normalizing the volume by letting $V = v_0^*/(\gamma/G)^2$ gives

$$\tan\theta^* = 0.72V^{1/7}. \tag{11}$$

For volume $v_0 > V$ other than those given in Eq. 11, the spherical cap solution is unstable. The solid line in Fig. 5

shows the theoretical bifurcation curve. In this comparison we have assumed that $\gamma = 73$ dyn/cm (the surface tension of water) and $G = 5 \times 10^3$dyn/cm, as described above. The theoretical curve captures the trends of the experiments.

Finally, we note that the shape of the colony close to the bifurcation point also follows from this analysis. The shape of the colony is $h(x) = h_0(x) + c\rho(x)$. A weakly nonlinear analysis around the bifurcation point demonstrates that if the volume of the colony increases from $v_0^* \rightarrow v_0^* + \delta v$, the solution is $c = (3\delta v/v''(1))$. To leading order in δv, the radius of the colony is constant.

Fig. 6 shows the two possible configurations for the colony near the bifurcation point, i.e., the spherical solution and the nonspherical solution. The inset shows the energy of both solutions as a function of distance from the bifurcation point. As advertised, the nonspherical solution has lower energy then the spherical one. Note that this comes about because the spherical solution has a larger radius (and hence higher surface area), to fit the constant contact angle condition.

DISCUSSION

We have demonstrated through experiments and a mathematical model that the shape of a growing yeast colony is governed entirely by surface energy minimization and surface adhesion when the colony is sufficiently small, but that above a critical volume elastic stresses play an equally important role in determining the colony shape. In the elastic regime, the colony shape is contact-angle-dependent. The role of elastic stresses in determining the contact-angle-dependent morphology is illustrated through a mathematical model, which demonstrates that above a critical (contact-angle-dependent) volume, the spherical-cap solution is unstable and elastic stresses are important. The contact angle dependence of the critical volume is quantitatively consistent with the experiments. Our mathematical analysis is limited to the neighborhood of the instability threshold. Beyond the threshold, there is a zoo of contact-angle-dependent colony shapes (e.g., the staircase morphology occurs when $\theta < 40°$, and when $\theta > 70°$ the colony has a single dimple in the center).

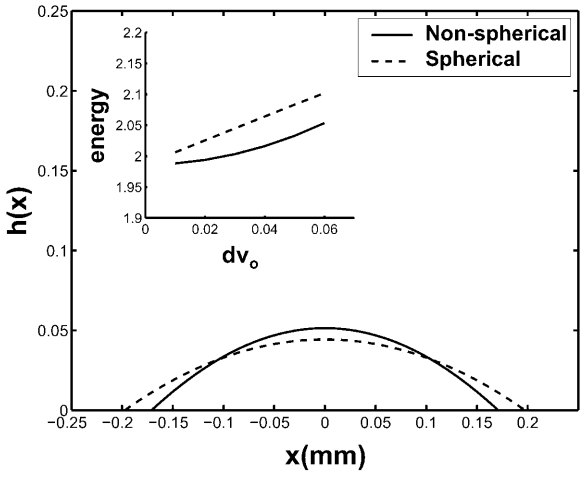

FIGURE 6 Theoretical solution and corresponding energy. Predicted nonspherical shape solution versus spherical cap solution for the same sample volume $v_0 = 0.5$, $\theta = 27.4°$, and $dv_0 = v_0/10$. Inset figure plots total energy as a function of dv_0, demonstrating that the nonspherical shape has lower energy.

The mathematical model that we have analyzed is phenomenological, in that it assumes that unbalanced capillary forces can be balanced by elastic stresses, although we do not give a microscopic description of how this coupling comes about. As an example, for the deformation of solid bodies, shape modulations of the crystal couple to elastic distortion through surface stresses, a concept that does not exist in our problem. One intriguing mechanism for the coupling is suggested by the striking similarity between our nonspherical morphologies and those that have been discovered in the shapes of a drying droplet of a colloidal suspension (Parisse and Allain, 1996). Although the humidity controlled environment of our experiments should not allow much drying to occur, the growth of the cells in the yeast colony implies that the volume fraction of solid particles in the colony is increasing. Such an increase cannot proceed indefinitely without dewetting the cells in the colony, resulting in elastic stresses. Further work analyzing the precise mechanisms and parameter regimes where such drying stresses could come about is underway.

The demonstration of elastic instability in this simple model of tissue growth points to the possibility of elastic effects in more complex situations. For example, the instability we have identified is the precursor to the complex morphologies discovered by Reynolds and Fink (2001). The precise role of elastic stresses in determining tissue morphologies under more general conditions remains to be seen. The present experience with yeast droplets demonstrates that at least two different materials with different adhesive energies are needed for an elastic instability. The general requirements for elastic stresses to play a role in determining tissue morphology remain to be worked out. It seems possible that the fundamental notion of selective adhesion as a driving force for tissue development needs to be supplemented with elastic effects. If so, there is the fascinating possibility of elastic stresses being regulated during development through, for example, cells modifying their individual stiffness.

We gratefully acknowledge Todd Reynolds and Gerald Fink for the supply of yeast samples, Elena Budrene, Gerald Fink, and Todd Reynolds for helpful discussions, and L. Mahadevan for incisive criticisms and comments. We thank Thucquyen Nguyen and Jeff Chabot for critical comments on the manuscript.

This work was supported by National Institutes of Health grant R01 GM 63618-01, and by the Division of Mathematical Sciences of the National Science Foundation (to M.P.B.).

REFERENCES

Batchelor, G. 1973. An Introduction to Fluid Dynamics. Cambridge University Press, Cambridge, MA.

Fink, R., and D. R. McClay. 1985. Three cell recognition changes accompany the ingression of sea urchin primary mesenchyme cells. *Dev. Biol.* 107:66–74.

Forgacs, G., R. Foty, Y. Shafrir, and M. Steinberg. 1998. Viscoelastic properties of living embryonic tissues: a quantitative study. *Biophys. J.* 74:2227–2234.

Foty, R., G. Forgacs, C. Pfleger, and M. Steinberg. 1994. Liquid properties of embryonic tissues: measurement of interfacial tensions. *Phys. Rev. Lett.* 72:2298–2301.

Foty, R., C. Pfleger, G. Forgacs, and M. Steinberg. 1996. Surface tensions of embryonic tissues predict their mutual envelopment behavior. *Development.* 122:1611–1620.

Glazier, J., and F. Graner. 1993. Simulation of the differential adhesion driven rearrangement of biological cells. *Phys. Rev. E.* 47:2128.

Landau, L., and E. Lifshitz. 1986. Theory of Elasticity. Pergamon Press, Oxford, UK.

Landau, L., and E. Lifshitz. 1987. Fluid Mechanics. Pergamon Press, Oxford, UK.

Larson, R. 1999. The Structure and Rheology of Complex Fluids. Oxford University Press, Oxford, UK.

Palsson, E., and H. Othmer. 2000. A model for individual and collective cell movement in *dictyostelium discoideum*. *Proc. Natl. Acad. Sci. USA.* 97:10448–10453.

Parisse, F., and C. Allain. 1996. Shape changes of colloidal suspension droplets during drying. *J. Phys. II Fr.* 6:1111–1119.

Reynolds, T., and G. R. Fink. 2001. Bakers' yeast, a model for fungal biofilm formation. *Science.* 291:878–881.

Ryan, P., R. A. Foty, J. Kohn, and M. Seinberg. 2001. Tissue spreading on implantable substrates is a competitive outcome of cell-cell versus cell-substratum adhesivity. *Proc. Natl. Acad. Sci. USA.* 98:4323–4327.

Smith, A., Z. Zhang, C. R. Thomas, K. E. Moxham, and A. P. J. Middleberg. 2000. The mechanical properties of *Saccharomyces cerevisiae*. *Proc. Natl. Acad. Sci. USA.* 97:9871–9874.

Steinberg, M. 1962. Mechanism of tissue reconstruction by dissociated cells. II. Time-course of events. *Science.* 137:762–763.

Steinberg, M. 1964. The problem of adhesive selectivity in cellular interactions. *In* Cellular Membranes in Development. M. Locke, editor. Academic Press, New York.

Townes, P. L., and J. Holtfreter. 1955. Directed movements and selective adhesion of embryonic amphibian cells. *J. Exp. Zool.* 128: 53–120.

Trinkaus, J. 1963. The cellular basis of *fundulus epiboly*. Adhesivity of blastula and gastrula cells in culture. *Dev. Biol.* 7:513–532.